JOURNAL OF GEOPHYSICAL RESEARCH, VOL. 100, NO. D6, PAGES 11,611–11,622, JUNE 20, 1995

Parameterization of the solar radiative characteristics of low clouds and studies with a general circulation model

C.-T. Chen[1] and V. Ramaswamy

Atmospheric and Oceanic Sciences Program, Princeton University, Princeton, New Jersey

Abstract. A broadband parameterization that improves the quantitative estimates of the solar radiative characteristics of low clouds is developed using reference solutions. The accuracy of the parameterization in determining the shortwave cloud absorption for a wide variety of low-cloud conditions is better than 20%. Other broadband treatments, which do not adequately account for the influences due to above- and in-cloud water vapor and water drop extinction, are also considered to investigate the sensitivity to these factors. The computed northern hemisphere summertime fluxes reveal that (1) the absorbed solar flux in low clouds (F_{abs}) is overestimated at high latitudes if the effect of attenuation by the above-cloud vapor is ignored in the determination of the water drop absorption, (2) F_{abs} is underestimated in the tropical regions if in-cloud vapor absorption is not considered, and (3) the conservative scattering assumption for drops yields a substantial underestimate of F_{abs} at most latitudes. General circulation model simulations with fixed sea surface temperatures and cloud amounts further highlight the significance of the vapor and drop optical properties. Differences in the broadband treatment of the radiative interactions with vapor and drops in low clouds introduce changes in the solar fluxes absorbed by the atmosphere and the surface; for the cases considered here, the solar flux change at the top of the atmosphere differs in sign from that at the surface. The flux differences bring about changes in vertical motion and precipitation; these, in turn, are accompanied by perturbations in the various components of the land surface heat (e.g., latent and sensible heat losses) and moisture (e.g., soil moisture, evaporation) budgets. For approximately similar solar flux differences the changes in the vertical motion, precipitation, and land surface parameters are dissimilar in the tropical and the midlatitude continental regions. Thus because of the adjustments in the atmosphere and the coupling between the atmosphere and the land surface processes, solar flux differences due to biases or deficiencies in the radiative treatment of vapor and drops affect the simulation of the hydrologic fields and the heat balance, including the atmospheric and land surface temperatures.

1. Introduction

The solar radiative interaction with water drops and vapor in the cloudy atmospheres of general circulation models (GCMs) is traditionally treated using broadband methods. For example, broadband parameterizations of *Lacis and Hansen* [1974, hereinafter referred to as LH] and *Slingo* [1989] are used for calculating the solar flux scattered and absorbed by clouds in several GCMs. An important general concern with broadband treatments is the need to satisfactorily account for the complicated spectral details of the near-infrared solar interactions, such as the effect of drop scattering on the water vapor absorption inside the cloud and that due to the overlap of the water vapor and drop absorption bands [*Ramaswamy and Freidenreich*, 1992, hereinafter referred to as RF2]. These interactions involve the convolution of the spectrally dependent values of three different physical entities: (1) the solar irradiance, (2) the absorption features of the water vapor molecule, and (3) the single-scattering properties of water drops.

In this study, high-spectral-resolution results for overcast skies are determined corresponding to a range of atmospheric situations. The reference results are then used to develop and test the accuracy of simple empirical expressions for the transmission and reflection by low-cloud layers (section 2). Section 3 compares the zonal mean solar fluxes obtained using the new parameterization with those from three other broadband treatments and thereby examines the radiative effects due to vapor and drops. Section 4 discusses the sensitivity of the atmosphere and land surface simulations in a GCM to different solar broadband treatments of low clouds. Analyses of the GCM experiments highlight the roles of the drop and vapor optical properties and the influence of their solar spectrum interactions upon the surface-atmosphere system. Section 5 summarizes the findings of this study.

2. Methodology for New Broadband Parameterization

Ramaswamy and Freidenreich [1991, hereinafter referred to as RF1] developed a technique to compute the near-

[1]Now at Max Planck Institute for Meteorology, Hamburg, Germany.

Paper number 95JD00590.
0148-0227/95/95JD-00590$05.00

infrared interaction of water vapor absorption and cloud extinction by approximating the scattering process with the delta-Eddington (DE) method [*Joseph et al.*, 1976], while maintaining the line-by-line (LBL) structure of water vapor absorption (for details on the method the reader is referred to the VC2 technique described by RF1; we will refer to it as the LBL + DE method in this paper). We employ this method for generating the reference results for overcast skies. The spectral interval 0–18000 cm^{-1} (wavelengths longer than 0.55 μm) is the basis for the broadband parameterization. The insolation in this interval is 966 W m^{-2}. The single-scattering properties of the water drops are described in terms of the cloud liquid water path (LWP) and effective drop radius (r_e) [*Slingo*, 1989].

RF2 showed that the broadband treatments of the spectrally dependent absorption due to drop and vapor inside the cloud and the spectral attenuation by the vapor above the cloud affect the accuracy of the cloud reflection and transmission, particularly for low clouds. The quantities that have a direct effect on the broadband cloud layer solar radiative properties, besides cloud LWP and r_e, are water vapor inside the cloud, water vapor above the cloud, solar zenith angle θ_0, and surface albedo α_{sfc}. While the range of possible values for each of the above parameters is vast, we attempt to reduce the number of variables and thereby construct an empirical parameterization for the radiative properties of cloud layers in the lower troposphere.

We assume the cloud r_e to have a nominal value of 10 μm. Since most clouds in the lower troposphere exhibit a droplet mode radius between 5 and 15 μm [*Mason*, 1971; *Stephens*, 1979], the r_e chosen is probably reasonable for the low-lying water clouds, which are the focus of this study. The solar zenith angle is assumed to be 53°; this is an approximate intermediate value of the solar zenith angle. A zero surface albedo is assumed; this simplifies the multiple-scattering effects by excluding the reflected upward flux from the surface. All the cloud layers considered in the calculations have their cloud tops fixed at 800 mbar since our aim is to have a parameterization for low-lying water clouds. The fixed cloud top level restricts the range of the impact due to the water vapor above the cloud (RF2) by assuming it to be nearly a constant; this further reduces the number of variables to be considered in the parameterization. In view of the above considerations, only two parameters remain as variables, namely, cloud optical depth and the in-cloud water vapor. Subsequently, we test the parameterization to variations in various parameters.

We assume that the broadband transmissivity of a cloud layer consisting of water drops and vapor can be obtained by the transmissivity of the water droplets multiplied by a factor, termed here as "VFT." VFT accounts for the effect of water vapor absorption inside the cloud. It also accounts for the differences in the details of the spectral interactions between the reference (LBL + DE) and the broadband drop radiative properties derived here. Thus we write

$$\mathrm{VFT}(\tau_{\mathrm{drop}}, W) = \frac{T_{\mathrm{LBL+DE}}(\tau_{\mathrm{drop}}, W)}{T_{l,\mathrm{drop}}(\tau_{\mathrm{drop}})} \tag{1}$$

where

$$T_{l,\mathrm{drop}}(\tau_{\mathrm{drop}}) = T_{0,\mathrm{drop}}(\tau_{\mathrm{drop}})\left(\frac{T_{l,\mathrm{drop}}}{T_{0,\mathrm{drop}}}\right)_{\theta_0=53°} \tag{2}$$

The various quantities in (1) and (2) are identified below.

$T_{\mathrm{LBL+DE}}$ cloud layer transmissivity calculated using the LBL + DE method;
$T_{l,\mathrm{drop}}$ drop transmissivity calculated using the solar spectral irradiance at cloud top;
$T_{0,\mathrm{drop}}$ drop transmissivity calculated using the solar spectral irradiance at the top of the atmosphere;
τ_{drop} drop optical depth;
W water vapor amount inside cloud layer.

$T_{0,\mathrm{drop}}$ is calculated following *Slingo* [1989] and represents the transmissivity as if there were no water vapor above or inside the cloud and with only drops being present in the atmosphere. In (2) the ratio $(T_{l,\mathrm{drop}}/T_0,\mathrm{drop})$ is used to obtain the drop transmissivity appropriate at the cloudtop level; this implicitly includes the effect of water vapor attenuation above the cloud. The ratio can be written as

$$\left(\frac{T_{l,\mathrm{drop}}}{T_{0,\mathrm{drop}}}\right)_{\theta=53°} = \frac{\int_{\Delta\nu} T_{0,\mathrm{drop}}(\nu)S_l(\nu)\,d\nu}{\int_{\Delta\nu} T_{0,\mathrm{drop}}(\nu)S_0(\nu)\,d\nu}\,\frac{\int_{\Delta\nu} S_0(\nu)\,d\nu}{\int_{\Delta\nu} S_l(\nu)\,d\nu} \tag{3}$$

where S_0 is the insolation at the top of the atmosphere and S_l is the solar flux incident at the top of the cloud layer. The calculation is performed with the solar zenith angle fixed at 53°.

Similarly, the reflectivity of the cloud layer is assumed to be the broadband reflectivity of the cloud droplet multiplied by another factor "VFR," which is analogous to VFT,

$$\mathrm{VFR}(\tau_{\mathrm{drop}}, W) = \frac{R_{\mathrm{LBL+DE}}(\tau_{\mathrm{drop}}, W)}{R_{l,\mathrm{drop}}(\tau_{\mathrm{drop}})} \tag{4}$$

$$R_{l,\mathrm{drop}}(\tau_{\mathrm{drop}}) = R_{0,\mathrm{drop}}(\tau_{\mathrm{drop}})\left(\frac{R_{l,\mathrm{drop}}}{R_{0,\mathrm{drop}}}\right)_{\theta_0=53°} \tag{5}$$

The relevant quantities in (4) and (5) are identified below.

$R_{\mathrm{LBL+DE}}$ cloud layer reflectivity calculated by using the LBL + DE method;
$R_{l,\mathrm{drop}}$ drop reflectivity calculated using the solar spectral irradiance at cloud top;
$R_{0,\mathrm{drop}}$ drop reflectivity calculated using the solar spectral irradiance at the top of the atmosphere.

$(R_{l,\mathrm{drop}}/R_{0,\mathrm{drop}})$ can be written in a manner analogous to (3):

$$\left(\frac{R_{l,\mathrm{drop}}}{R_{0,\mathrm{drop}}}\right)_{\theta=53°} = \frac{\int_{\Delta\nu} R_{0,\mathrm{drop}}(\nu)S_l(\nu)\,d\nu}{\int_{\Delta\nu} R_{0,\mathrm{drop}}(\nu)S_0(\nu)\,d\nu}\,\frac{\int_{\Delta\nu} S_0(\nu)\,d\nu}{\int_{\Delta\nu} S_l(\nu)\,d\nu} \tag{6}$$

Note that VFT and VFR are not only functions of the amount of vapor inside the cloud but also depend on the drop

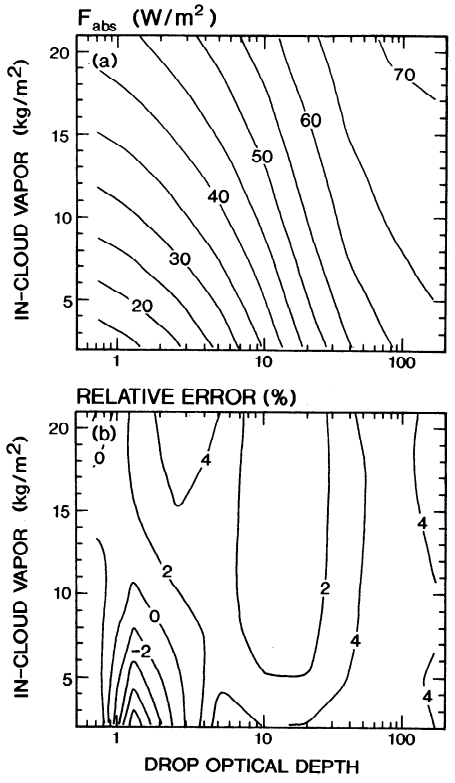

Figure 1. (a) Reference results and (b) the relative accuracy of the solar flux absorbed within low-cloud layers due to the new parameterization, as a function of cloud drop optical depth and in-cloud vapor amount.

optical depth since the multiple scattering by the droplets enhances the absorption by the vapor. The transmissivity (equation (2)) and reflectivity (equation (5)) of cloud drops are calculated using the solar spectral irradiance incident at the top of the cloud layer, instead of at the top of the atmosphere.

$(T_{l,\mathrm{drop}}/T_{0,\mathrm{drop}})_{\theta_0=53°}$ and $(R_{l,\mathrm{drop}}/R_{0,\mathrm{drop}})_{\theta_0=53°}$ are calculated using the reference values of downward solar fluxes at the top of the atmosphere and at the top of the cloud, as appropriate for a solar zenith angle of 53°. The single-scattering properties considered correspond to the spectral bands 8 to 24 of *Slingo* [1989]. For wavelengths longer than 4 μm (which was not included in Slingo's tabulation), the drop single-scattering parameters are obtained in the same way as in RF2.

The atmospheric profile used for constructing the parameterization is the midlatitude summer atmosphere [*McClatchey et al.*, 1972], with water vapor as the only gaseous absorber. Nine cloud drop optical depths τ_{drop} are chosen. The range of τ_{drop} is from 0.625 to 160. Most τ_{drop} values of low clouds are likely to be within this range [*Rossow and Lacis*, 1990]. The in-cloud vapor W depends on the cloud geometrical layer thickness chosen. The vapor is always assumed to be at its saturated value in the cloud layers. Eight different geometrical thicknesses (800–820 to 800–960 mbar) are considered. The corresponding water vapor amounts for these eight thicknesses are 2.26 to 20.85 kg m^{-2}. There are, thus, a total of 72 cloud cases, covering a wide range of τ_{drop} and W combinations for low-lying clouds.

The empirical factors VFT and VFR are determined using (1)–(6) and are represented by a polynomial series in τ_{drop} and W (Appendix). The relative errors in the fits are less than 1%. VFT and VFR range in values from 0.74 to 1 and from 0.95 to 1, respectively, implying that the vapor effects and the broadband aspect of the parameterization reduce the cloud transmissivity and reflectivity compared to the case when only drops are considered.

We consider next the application of our parameterization to the broadband treatment of solar radiative transfer in vertically inhomogeneous overcast atmospheres. The products VFT(τ_{drop}, W) ($T_{l,\mathrm{drop}}(\tau_{\mathrm{drop}})$) and VFR($\tau_{\mathrm{drop}}$, W) ($R_{l,\mathrm{drop}}(\tau_{\mathrm{drop}})$) yield the near-infrared fluxes transmitted and reflected, respectively, by the cloud layer consisting of drops and vapor. If the broadband attenuation by vapor in the other atmospheric layers is given by some appropriate formulation, then the cloud layers and the vapor-only layers of the atmosphere can be combined by the usual "adding" method [e.g., *Coakley et al.*, 1983]. In this work we use the modified LH method to compute the absorption due to the vapor outside of the cloud (RF2). Because of the use of this scheme, the incident solar downward flux at the top of a low cloud becomes slightly different from that obtained using the LBL + DE method. However, the difference between the two schemes is <2% for a zenith angle of 53°, indicating that this is not an important issue.

The one-dimensional broadband radiative transfer model for the vertically inhomogeneous atmosphere is the same as in the work of *Ramaswamy and Chen* [1993, hereinafter referred to as RC], with the exception of the new cloud radiative parameterization. Low cloud is the only cloud type assumed for present purposes while surface albedo is zero. The incident solar flux at the top of the atmosphere is 579 W

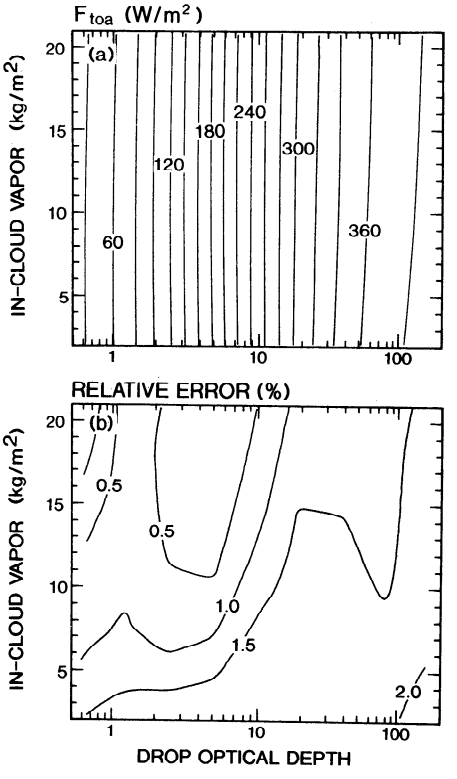

Figure 2. As is Figure 1 except for the upward solar flux at the top of the atmosphere.

Table 1. Reference Computations of Absorbed Flux (W m^{-2}) in Clouds and Relative Errors (%) Using the New Parameterization

Case	$\tau_{drop} = 1$		$\tau_{drop} = 10$		$\tau_{drop} = 100$	
	W m^{-2}	%	W m^{-2}	%	W m^{-2}	%
$\theta_0 = 0$	50.2	3	98.1	−5	145.8	2
$\theta_0 = 75$	13.3	9	14.4	17	20.0	12
$r_e = 5$ μm	30.6	−2	40.8	−11	53.1	−3
$r_e = 15$ μm	33.2	4	56.0	7	79.8	10
$\alpha_{sfc} = 0.1$	33.1	−1	49.8	1	67.6	6
$\alpha_{sfc} = 0.8$	41.2	−12	57.6	9	68.9	10
900- to 920-mbar cloud	10.5	18	31.5	14	55.9	11
600- to 900-mbar cloud	78.2	−29	87.0	−18	88.9	−1
SAW atmospheric profile	20.0	−48	44.4	−14	73.3	−8
TRP atmospheric profile	31.6	18	47.7	9	65.2	10

Results are obtained for three drop optical depths (cited for the visible spectrum) and for conditions that represent departures from the nominal case. The nominal case is the midlatitude summer profile, with $r_e = 10$ μm, solar zenith angle $\theta_0 = 75$, surface albedo $\alpha_{sfc} = 0.0$. SAW and TRP denote subarctic winter and tropical profiles, respectively.

m^{-2} (0–18000 cm^{-1} spectrum) for a zenith angle of 53°. The accuracies of the fluxes absorbed by the cloud, reflected at the top of the atmosphere, and transmitted to the surface are shown in Figures 1, 2, and 3, respectively, for various drop optical depths and in-cloud vapor amounts.

Figure 1 shows the reference value and the relative errors in the absorbed solar flux within cloud layers (F_{abs}). As expected, F_{abs} increases with drop optical depth and in-cloud vapor amount (Figure 1a). The relative errors in F_{abs} with the new parameterization are less than 5% in most cases (Figure 1b). The upward solar flux at the top of the atmosphere (F_{toa}) increases with drop optical depth (Figure 2a). It also decreases slightly with an increase in water vapor amount inside the cloud. The relative errors in F_{toa} are less than 2% (Figure 2b). The downward solar flux at the surface (F_{sfc}) decreases with increasing drop optical depth and, to a lesser extent, with increasing in-cloud vapor amount (Figure 3a). Though the relative errors in F_{sfc} exceed 10% for larger drop optical depths (Figure 3b), the absolute values of the errors are less than 5 W m^{-2}.

As stated earlier, the empirical broadband parameterization has been deduced using a fixed value of solar zenith angle, effective radius, surface albedo, atmospheric profile, and low-cloud geometrical thicknesses less than 160 mbar. We perform a limited number of sensitivity tests to determine the error in F_{abs} when conditions different from the above are considered (see *Chen* [1994] for more details). Table 1 lists the reference value and the relative errors under different conditions. In each case, except for the variable under consideration, all other parameters assume nominal values as stated earlier. There are some cases with relative errors exceeding 15%. However, the absolute errors are less than 10 W m^{-2}, except when the cloud is located between 600 and 900 mbar and the drop optical depth is less than 10. Thus the empirical parameterization, with an explicit dependence on only two variables, should yield reasonably accurate results for a variety of low-lying cloud cases.

3. Comparisons With Other Broadband Parameterizations and Zonal Mean Differences

3.1. Other Broadband Parameterizations

To place the new parameterization in perspective and to highlight the characteristics of the solar vapor-drop interactions, we consider other methods proposed in the literature and compare them with that developed here.

Method I (same as technique A in RF2) uses a *Slingo* [1989] type formulation to determine the cloud radiative properties and ignores the influences due to the above-cloud vapor absorption on the computation of the broadband drop reflection and transmission. It also ignores in-cloud vapor absorption.

Method II (same as technique B in RF2) assumes that the cloud layer reflection is independent of the in-cloud vapor. The total transmission by the cloud layer is assumed to be the product of two separate transmission functions: the transmissivity of the drops and that due to vapor; but, like method I, it ignores the effect of the above-cloud vapor on the determination of the broadband drop radiative properties. The effect of drop multiple scattering on the enhancement of the absorption by the in-cloud vapor is also excluded.

Method III, which has its origins in LH, is similar to II, except now the cloud droplets are considered to be pure scatterers. Only in-cloud water vapor absorption is assumed to contribute to the cloud layer absorption. Method IV employs the new broadband parameterization.

From the RF2 study, the water vapor inside and above cloud have distinct impacts on cloud layer absorption. Neglect of the former underestimates the cloud layer absorption, while neglect of the latter serves to overestimate the drop absorption by considering an increased solar flux incidence at the cloud top.

3.2. Comparative Accuracy of the Zonal Mean Solar Fluxes

We compare the latitudinal distribution of the solar fluxes obtained from using the four different parameterizations. In contrast to the previous section we now consider three levels of clouds, the entire solar spectrum, and a GCM's zonal mean climatology. The effective drop radius (r_e) is assumed to be 10 μm for all clouds. The cloud liquid water paths (LWPs) for high, middle, and low clouds are fixed at 0.007, 0.025, and 0.08 kg m^{-2}, respectively. The choice of LWP and r_e considered yields a low-cloud drop optical depth of 12.7. Latitudinally dependent cloud amounts and heights, atmospheric profiles, and surface properties are the same as

in the VIZSC experiment described in RC and constitute the "control" climatology of a R15 GCM [*Manabe and Broccoli*, 1985]. The low-cloud cover ranges from 14% to 75% (RC), with most of the tropical regions having a 30% cloud amount. The solar radiative algorithm employed is the same as in the Manabe-Broccoli study, with the radiative effects of carbon dioxide and ozone included. The solar radiative properties of middle and high clouds are determined using the *Slingo* [1989] formulation and the delta-Eddington method [*Joseph et al.*, 1976] for drops; that is, $R_{0,\text{drop}}$ and $T_{0,\text{drop}}$, as discussed in section 2, are computed for these clouds and assumed to represent the cloud properties. Note that vapor effects are less important for the solar radiative properties of high and middle clouds. The reflectivity and transmissivity of the low clouds are determined according to each of the four methods. The cloud reflection and transmission are calculated in the UV and visible using bands 1–10 in *Slingo*'s [1989] table and, in the near infrared, using bands 11–24. VFT and VFR are assumed to be 1 for the (visible) spectral range $\geq$18000 cm^{-1} (i.e., the above-cloud and in-cloud vapor do not affect the drop reflection and transmission, since water vapor possesses negligible absorption in this range).

The zonal mean solar radiative fluxes depend on the available insolation, water vapor, and cloud cover. For example, the equatorial region has a total solar (visible plus near infrared) insolation of about 420 W m^{-2} throughout the year, while at midlatitudes it is 500 W m^{-2} during summer. There is more moisture in the summer hemisphere than in the winter hemisphere. The existence of the high and middle clouds reduces the sensitivity due to low-cloud properties. Higher surface albedo in the polar regions also reduces the sensitivity of the Earth-atmosphere system to the solar radiative effect of low clouds (RC).

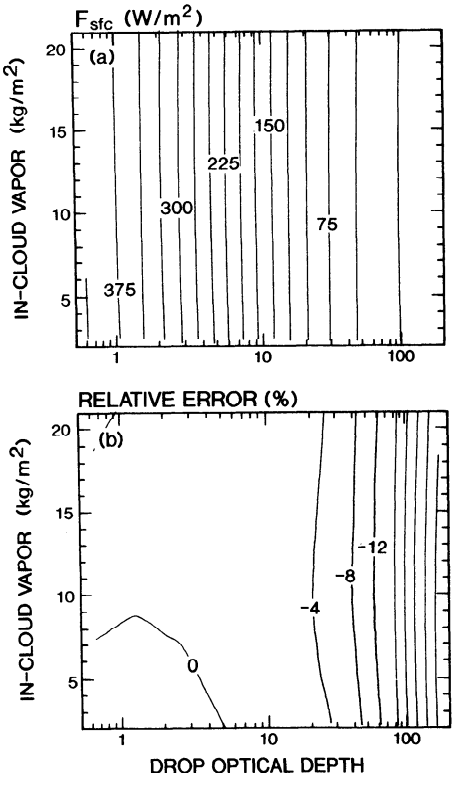

Figure 3. As is Figure 1 except for the downward solar flux at the surface.

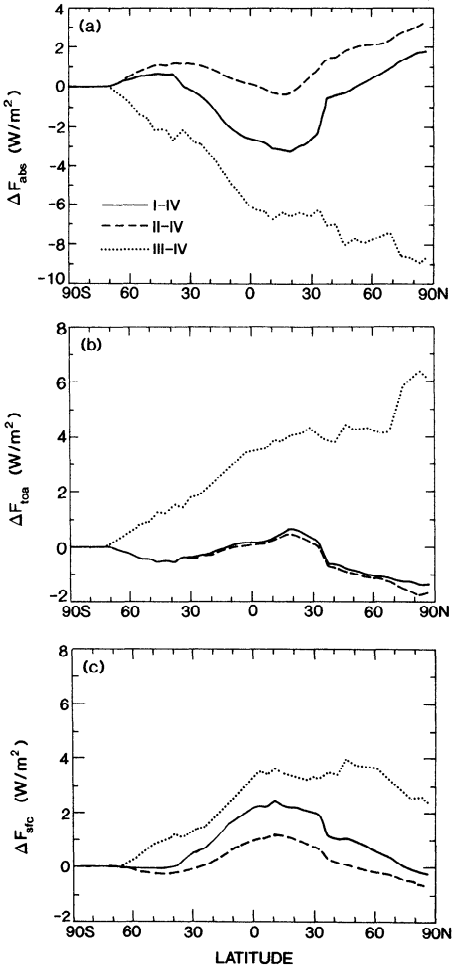

Figure 4. Differences (June, July, August averages) in the zonal mean solar flux (W m^{-2}) (a) absorbed by the cloud (F_{abs}), (b) reflected at the top of the atmosphere (F_{toa}), and (c) net transmitted to the surface (F_{sfc}), between methods I and IV, II and IV, and III and IV, respectively.

We examine the differences in the zonal mean fluxes between the new parameterization (method IV) and each of the other methods during the northern hemisphere summertime (June, July, August). Figure 4a shows the differences in the zonal mean flux absorbed by the low-cloud layer (F_{abs}). The in-cloud water vapor amount is relatively small for the high-latitude clouds (<10 kg m^{-2} poleward of 50°). Ignoring the solar flux absorption by the in-cloud vapor at the high latitudes has less influence on F_{abs} than neglect of above-cloud vapor, resulting in an overestimate of F_{abs} in these regions. Thus method I yields a larger F_{abs} in high latitudes. On the other hand, for the tropical region the low cloud contains a relatively higher in-cloud vapor amount (between 20 and 30 kg m^{-2}). The underestimate of cloud absorption due to a neglect of the absorption by in-cloud water vapor exceeds the effect of not accounting for the above-cloud vapor absorption in the computation of the drop properties. Thus a decrease in F_{abs} is obtained near the equator.

F_{abs} from method II exceeds IV at all latitudes. The difference is mainly due to the overestimate in F_{abs} which arises because of not considering the influence of the vapor

absorption above the cloud on the broadband drop radiative properties. The overestimate is less in the tropics because the enhancement in the in-cloud vapor absorption due to the increase in drop multiple scattering, which is implicitly incorporated in method IV, is not included in II. In contrast to I, method II absorbs 3 W m^{-2} more near the equator and about 1 W m^{-2} more in midlatitudes. Method III, which assumes the drops to be nonabsorbing, yields less cloud layer absorption than IV. The relative errors are larger (>6 W m^{-2}) when the in-cloud vapor is small and thus has a lesser role in absorption (i.e., middle and high latitudes in the summer hemisphere).

Figure 4b shows the differences in the zonal mean upward solar fluxes at the top of the atmosphere (F_{toa}). F_{toa} from method I is less than IV, except in the northern tropical regions. This is because, in general, the cloud drop reflectivities in I, which do not account for the above-cloud vapor absorption of the direct beam, are smaller than for method IV (RF2). However, between 30°N and 30°S the differences in F_{toa} are smaller than at the higher summer latitudes. This is because method I does not, in addition, include the decrease in the drop reflectivity caused by the effect of in-cloud vapor absorption, i.e., the factor VFR in method IV. VFR is greater in the tropical regions where in-cloud vapor amounts are larger. This causes the difference in F_{toa} between I and IV to be reduced. The additional considerations in method II relative to I do not alter the difference vis-à-vis IV. F_{toa} for method III exceeds IV because the conservative scattering assumption increases the drop reflectivity. A large increase (more than 4 W m^{-2}) occurs in the polar region of the northern hemisphere where more insolation is available and less in-cloud vapor is present.

Figure 4c shows the differences in the zonal mean net solar fluxes at the surface (F_{sfc}). Ignoring in-cloud vapor absorption in method I allows more flux to go through the cloud. Therefore even though the influence of the above-cloud vapor on the broadband drop transmission (RF2) is ignored, the difference between I and IV still turns out to be positive for clouds containing large amount of in-cloud vapor (between 60°N and 30°S). For clouds with less in-cloud vapor, e.g., summer polar regions, the lack of accounting of the above-cloud vapor attenuation becomes a more important factor than the exclusion of in-cloud vapor absorption, resulting in a negative I–IV there.

The in-cloud vapor path increase due to multiple scattering by drops is not accounted for in method II. F_{sfc} from method II is more than IV between 40°N and 20°S. This is mainly due to the neglect of the in-cloud vapor in the multiple-scattering process. In the rest of the globe the smaller apparent drop transmissivity of II, due to the above-cloud vapor not being accounted for (RF2), plays a more important role than the in-cloud vapor path. The pure scattering assumption of drops in method III yields an increase in drop transmissivity and thus leads to overestimates in the surface flux. This is particularly so near the equator and at 50°N where higher insolation and/or larger in-cloud vapor amounts prevail. In the polar region, the high surface albedo reduces the sensitivity of the net solar flux change (RC).

The differences in cloud layer absorption, reflection, and transmission between the methods discussed above depend on the drop optical depth assumed. To study the sensitivity to other drop optical depths, we repeated the above experiments for methods I, II, III, and IV with low-cloud liquid water paths one tenth and 10 times that assumed in the above calculations (i.e., 0.008 and 0.8 kg m^{-2}, respectively, implying order of magnitude changes in drop optical depth). The globally and annually averaged flux results [*Chen*, 1994] indicate that the differences in F_{abs} can reach 10 W m^{-2}, that in F_{toa} can be as high as 8 W m^{-2}, while that in F_{toa} can attain values up to 3 W m^{-2}. The differences between methods I and III, III and IV, and I and IV tend to be the highest.

The results demonstrate the marked sensitivity of the zonal mean fluxes to different broadband treatments of in-cloud and above-cloud vapor and drop properties. An additional appreciation is obtained by noting that the flux differences are comparable to those due to changes in trace gas amounts. The sensitivity arises because both vapor and drops assume important roles in governing the solar fluxes at the surface, at the top of the atmosphere, and that absorbed within the atmosphere. It is also apparent that the sign of the flux change at the surface between various treatments of vapor-drop solar interactions can differ from that for the surface-atmosphere system (Figure 4).

4. Effect of Different Broadband Parameterizations on GCM Simulations

It is of interest to set a broader context and inquire into the roles of vapor and drops and the impacts due to the different solar treatments of low-cloud vapor-drop radiative interaction on the general circulation. We employ a nine-level R15 Geophysical Fluid Dynamics Laboratory GCM [*Manabe and Broccoli*, 1985] whose control climatology was used in section 3. To simplify the scope, we investigate the effects over land surfaces only, with the sea surface temperatures, sea ice, and cloud distributions fixed as per the GCM's control climate. The cloud distributions are the same as in section 3. Low-cloud shortwave radiative treatments according to methods I, III, and IV are employed in succession. The radiative transfer algorithm is the same as in the earlier GCM study. In the longwave, clouds are assumed to be "black." For each method the GCM is run for 20 years. The resulting equilibrium thermal and hydrological model responses of the land areas are examined by taking the averages of the last 10 years of the runs.

We analyze the results by composing two sets of differences. First, the results from method III are compared with method IV. This yields a perspective on the effect due to inaccuracies in the low-cloud radiative transfer parameterization and serves to illustrate the importance of considering the proper drop optical properties, particularly absorption, in the low-cloud layer. Second, we compare methods I and III, which contrasts the roles of in-cloud vapor absorption and drop extinction. In both cases the difference in the solar fluxes can be viewed as perturbations and the differences in the GCM simulations can be taken to be the responses to the perturbations. Figure 4 indicates that the change in the flux at the top of the atmosphere (i.e., absorbed within the surface-atmosphere system) in methods III–IV and I–III is of the opposite sign to that at the surface.

We focus on the response of the atmosphere and the land surface heat and water budgets during the northern summer season. Three continental regions, as shown in Figure 5, are chosen for examining the changes. Regions "US," "EA,"

and "NA" represent the United States (~35°–60°N), Europe and western Asia (~40°–60°N), and northern Africa (~10°–30°N), respectively.

To discern the basic climate of the model, Table 2 lists the summertime (June, July, August) area-averaged equilibrium thermal and hydrological fields for method IV. The sign convention adopted here is such that the components of the heat budget are positive if they heat the surface. A negative value indicates a cooling of the surface. Also, if a term is a source of water for the surface, then it is positive, while if it is a sink, it is negative. The sign of the changes in the source terms for energy and moisture is positive if they increase. The sign of the changes in the sink terms is also positive if they decrease. Table 2 indicates that the heat and water balances of the three regions are very different depending on the ambient moisture, especially soil moisture which directly affects the amount of evaporation. NA is somewhat dry during summer. Though both US and EA are in the midlatitudes, EA has a relatively dry summer season. The standard deviation of the summer surface temperature for the US, EA, and NA regions are 0.6, 0.4, and 0.5 K, respectively.

4.1. Methods III–IV

Methods III and IV yield a zonal mean solar flux difference at the top of the atmosphere ($SW_{toa,i}$) of ~4 W m^2 over each region (Table 3); that is, the net solar flux absorbed by the surface-atmosphere system in III is less than in IV. The difference is comprised of a rearrangement of the solar fluxes absorbed by the atmosphere and the surface, with a decrease in the former and an increase in the latter over all three regions. Comparing method III with IV, the simulated summer surface temperature (T_{sfc}) changes for US, EA, and NA are −0.8, −1.9, and −0.2 K, respectively (Table 3). Though the solar flux changes at the surface and the top of the atmosphere in the three regions are approximately similar, the changes in the parameters in each region, including the decrease in T_{sfc}, are quite distinct. In EA, rainfall (R) and soil moisture (SM) increase. Since the evaporation (E) in the model depends on the amount of soil moisture (SM), the latent heat flux (LH) to the atmosphere increases in EA. The changes in sensible heat (SH) and longwave radiative fluxes (LW_{sfc}) restore the surface energy balance; these are associated with a reduction in T_{sfc}. The changes in rainfall, soil moisture, latent heat release, and T_{sfc} in the US region are similar to those in EA, except the magnitudes are less. Thus even along the same latitude belt, the response to a uniform solar flux perturbation can consist of nonuniform changes in the components of the surface energy and moisture budgets.

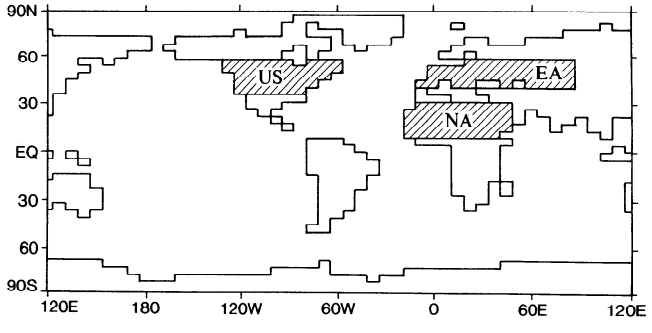

Figure 5. The location of the three regions selected for the examination of the area-averaged heat and water budgets in the general circulation model (GCM) experiments.

Table 2. Area-Averaged Thermal, Radiative, and Hydrological Fields in the GCM (June, July, August Averages) Obtained by Using the New Parameterization (Method IV)

	US	EA	NA
T_{sfc}, K	297	302	306
SW_{toa}, W m^{-2}	315	311	332
Surface Energy Budget			
SW_{sfc}, W m^{-2}	205	201	201
LW_{sfc}, W m^{-2}	−67	−89	−95
SH, W m^{-2}	−43	−72	−53
LH, W m^{-2}	−95	−40	−53
Moisture Fields			
E, m yr^{-1}	−1.20	−0.51	−0.66
SM, m	0.064	0.015	0.024
R, m yr^{-1}	1.20	0.31	0.89

GCM, general circulation model. US, EA, and NA denote the United States, Europe and Asia, and northern African regions, respectively. T_{sfc}, surface temperature, SW_{toa}; net (down minus up) solar flux at the top of the atmosphere; SW_{sfc}, net solar flux at ground; LW_{sfc}, net longwave flux at ground; SH, sensible heat flux; LH, latent heat flux; E, evaporation and sublimation; SM, soil moisture; R, rainfall. The sign convention is such that the components of the heat budget are positive if they heat the surface. A negative value indicates a cooling of the surface. Also, if a term is a source of water for the surface, it is positive, while if it is a sink, it is negative.

In NA there is a much smaller temperature reduction than in US and EA, even though the solar flux differences are similar. In the NA region the sense of changes in precipitation, soil moisture, evaporation, sensible and latent heat release are opposite to that in EA (Table 3). This result is similar to the reduction in precipitation and soil moisture found in a GCM study of the climate effects due to background tropospheric aerosols [*Coakley and Cess*, 1985]. A similar result is also found in a study of the climate effects due to changes in surface albedo [*Charney et al.*, 1977; *Lofgren*, 1993]. However, there are differences between the earlier works and methods III–IV. Specifically, in the present experiment, the partitioning of the solar flux difference between the surface and the atmosphere is different.

If we consider the Coakley-Cess study as an example, there is a solar radiative flux deficit at both the surface and the top of the atmosphere in that study. The simulated decrease in precipitation in that experiment is attributed to a decrease in the surface solar flux which suppresses convective activities, cools the atmosphere and surface, and reduces the surface latent heat and sensible heat losses. In methods III–IV, while there is a decrease at the top of the atmosphere, the surface solar flux in NA actually increases by 3.7 W m^{-2} (Table 3). In the present study, too, the solar deficit for the surface-atmosphere system induces a cooling tendency in NA (Figure 6); there is a suppression of the convective activity in the atmosphere as a whole and therefore a reduction in precipitation. The surface latent release is also reduced as in the earlier study. However, in contrast to the previous study, the III–IV case actually has an increase in the sensible heat flux loss owing to the surface being cooled less than the near-surface layers. Because of the atmospheric cooling and consistent with the relatively

Table 3. Changes in the GCM Area-Averaged Thermal, Radiative, and Hydrological Fields (June, July, August Averages) Obtained by Comparing Method III with IV and Method I With III

	Methods III–IV			Methods I–III		
	US	EA	NA	US	EA	NA
T_{sfc}, K	−0.8	−1.9	−0.2	1.4	1.6	−0.1
$SW_{toa,i}$, W m^{-2}	−4.1	−4.2	−4.0	4.9	5.0	3.6
Changes in the Surface Energy Budget						
SW_{sfc}, W m^{-2}	4.1	3.7	3.7	−3.3	−2.7	−1.8
LW_{sfc}, W m^{-2}	−0.8	2.9	−4.0	−0.7	−2.6	3.5
SH, W m^{-2}	−2.2	2.4	−5.2	1.0	−3.9	4.2
LH, W m^{-2}	−1.2	−9.1	5.6	3.0	9.2	−5.8
Changes in the Moisture Fields						
E, m yr^{-1}	−1.5	−11.4	7.0	3.8	11.6	−7.4
SM, cm	0.3	0.6	−0.3	−0.7	−0.7	0.4
R, m yr^{-1}	4.6	11.6	−10.9	−9.4	−10.9	14.4

Notation and the units in this table are the same as those used in Table 2, except for SM; $SW_{toa,i}$ is the initial solar net radiative flux difference at the top of the atmosphere, in contrast to the equilibrium values listed in the other rows. The sign of the change in the source terms for energy and moisture is positive if they increase. The sign of the changes in the sink terms is negative if they increase.

smaller surface temperature change, there is an increase in the surface net longwave energy loss. In general, the solar flux differences at the top of the atmosphere and surface in NA govern the change in rainfall, the atmospheric thermal profile, and the surface energy and moisture components.

There is a dissimilarity in the manner in which the midlatitude (US, EA) and the tropical (NA) atmospheric regions are affected by the solar flux differences. If the atmospheric changes due to the top-of-the-atmosphere solar flux deficits (Table 3) in each region consisted mainly of an adiabatic heating process, then a reduction in vertical velocity would be expected. The low-level convergence and the 500-mbar vertical velocity are indeed reduced in NA (by 0.016 μbar s^{-1}), a feature also seen in the Coakley-Cess study. Thus in the NA region the radiatively induced diabatic cooling of the atmosphere, as implied by III–IV, suppresses convection; this reduces the latent heat release within the atmosphere, contributing further to the diabatic cooling.

However, in EA and US the vertical velocities actually increase (by 0.004 and 0.012 μbar s^{-1}, respectively), indicating that there is adiabatic cooling instead of heating, accompanying the solar radiative deficit of III–IV. Thus compared to NA, changes in horizontal heat advection over both EA and US regions acquire a more important role in balancing the cooling. The increase in vertical velocity implies an increase of the latent heat release within the atmosphere which compensates, to some extent, the radiatively induced cooling. An increase in precipitation occurs which enhances the latent heat loss from the surface. The reduction of the adiabatic cooling in the tropics on the one hand and the importance of advective heating in the midlatitudes on the other is consistent with theory. Using a linear quasi-geostrophic model and scaling arguments, *Held* [1983] has argued that the primary mechanism balancing diabatic processes at midlatitudes is advection. Other GCM investigations of perturbations in the midlatitude and tropical regions also suggest a similar mechanism [*Lofgren*, 1993; *Coakley and Cess*, 1985].

There is an approximately similar cooling of the troposphere in all three areas (Figure 6) owing to the flux difference in F_{toa} (Table 3) being negative. However, for the boundary layer and surface, the temperature changes are more nonuniform owing to the manner in which the atmosphere and land surface processes respond in each region. Because of the larger surface cooling relative to NA the surface sensible and longwave heat losses are actually reduced in EA. The smaller surface cooling in US (compared to EA) is accompanied by a slight relative increase in the surface net longwave loss. While the surface temperature changes in US and EA (Table 3) exceed the model's standard deviation (~0.6 K), the response in NA is quite small and insignificant.

4.2. Methods I–III

The comparison of I–III represents the sensitivity to two different assumptions concerning low-cloud radiative prop-

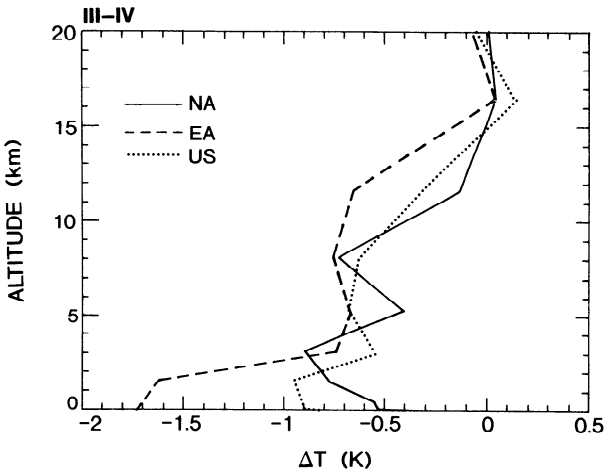

Figure 6. Changes in the GCM atmospheric temperature profile (June, July, August averages) over the NA, EA, and US regions (see Figure 5) for methods III–IV.

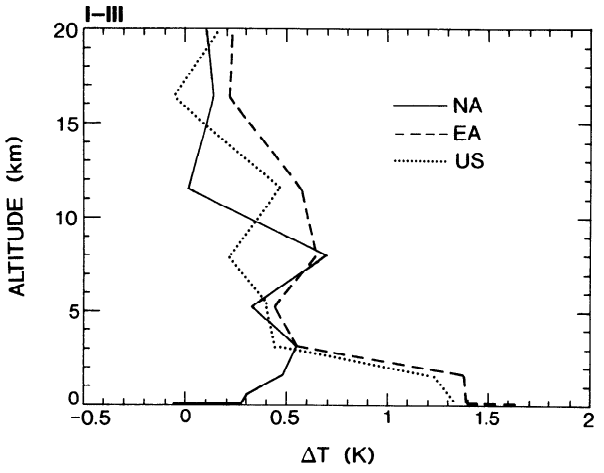

Figure 7. Same as Figure 6 except for methods I–III.

erties, namely, consideration of drop absorption only (method I) or vapor absorption only (III) inside the cloud layer. The radiative flux difference between I and III at the top of the atmosphere again has an opposite sign to that at the surface, as in III–IV (Table 3). However, in contrast to section 4.1, there is now an increase of the solar flux absorbed by the atmosphere, while at the surface, there is a decrease. Thus the difference cases I–III and III–IV constitute, qualitatively, a complementary pair. The reduction in the net solar flux at the surface and an increase in the top-of-the-atmosphere net solar flux over all three regions imply an increase in the diabatic heating. The solar radiative flux differences for the surface-atmosphere system in all the regions exceed 3.5 W m^{-2}, with those in US and EA being similar. As in III–IV, the responses in the various surface components differ for the three regions.

In the NA region the addition to the diabatic heating of the atmosphere (I–III) is accompanied by an increase in the low-level convergence and the vertical velocity at 500 mbar (by 0.021 μbar s^{-1}). There is thus an additional contribution to the diabatic heating due to an increase in convective activity and latent heat release within the atmosphere, leading to an increase of precipitation. At the surface, there results an increase in the latent heat loss. Owing to the warming of the atmosphere relative to the change at the surface (Figure 7), there is a reduction in the loss of longwave and sensible heat fluxes (Table 3). The results here are almost exactly opposite in nature to those seen earlier for III–IV. Note that the solar flux change at the top and at the surface are less in magnitude than some of the other terms in the surface energy balance.

In contrast to the tropics the change in the 500-mbar vertical velocity is actually one of a reduction, not an increase, in the extratropical regions EA and US (by 0.002 and 0.01 μbar s^{-1}, respectively). There is hence an adiabatic heating change accompanying the radiatively induced I–III diabatic heating of the atmosphere (Table 3). Compared to NA, the changes in the lower-tropospheric winds result in lesser alterations of the local convergence/divergence in both EA and US. For example, methods I–III indicate (not shown) that the equatorward and eastward winds in the EA region are strengthened; thus the advective cooling is enhanced. Thus for EA and US, too, the I–III adjustment is opposite in nature to that for III–IV. This feature, namely, the diabatic heating difference over the midlatitude continents being balanced by the strengthening of the equatorward surface winds is again consistent with the theoretical arguments of *Held* [1983] and the GCM experiments of *Lofgren* [1993]. As with the discussions concerning III–IV, this indicates that advective processes have acted to provide the balance in a relatively more important manner in the midlatitudes than in the tropics. The sense of the changes in the surface energy and moisture components for both EA and US are, in general, opposite to that in III–IV. In EA the reduction of the vertical velocity at 500 mbar is accompanied by a decrease in precipitation (Table 3), leading to surface dryness and a reduction in the surface latent heat flux release. The surface warming is accompanied by an increase in the surface net longwave radiative flux (Table 3).

The vertical profile of the temperature changes for I–III is shown in Figure 7. In all three regions the middle to upper troposphere warms, consistent with the sign of the F_{toa} changes (Table 3). However, as seen for III–IV, the responses in the surface temperature and in all components of the land surface energy and moisture budget are, in addition, dependent on the atmospheric and land surface adjustments, including the changes in vertical velocity and precipitation over the domain. As in III–IV, the surface temperature change in NA is small but exceeds the model's standard deviation (~0.6 K) in US and EA.

Finally, for methods I–III, we summarize the changes in the quantities involved in the heat and water budgets from the zonal mean perspective. These are illustrated in Figure 8. The solar radiative flux difference at the top of the atmosphere is >3 W m^{-2} in the northern hemisphere (Figure 8c). The change in T_{sfc} can exceed 1 K poleward of 40°N but is relatively small or even negative in the tropical region (Figure 8a). Near 10°N (which includes the NA region) a decrease in the surface temperature is associated with an increase in latent heat flux loss from surface (negative under our sign convention, Figure 8b) and a decrease in the sensible (Figure 8b) and the net upward longwave radiative flux losses (Figure 8c). At 50° and 70°N (which includes the EA and US regions), T_{sfc} increases (by about 1 K) and latent heat flux loss from surface decreases. The change of latent heat flux follows the change in evaporation, which, in turn, is affected by rainfall and soil moisture (Figure 8d).

Table 3 and Figures 4 and 6–8 point out that differences in the broadband determination of the vapor-drop solar interactions in low clouds, due to different treatments of drop and vapor optical properties, initiate flux changes at the surface and in the surface-atmosphere system. Thus the solar absorption within the atmosphere and by the surface is altered. This, in turn, causes changes in the adiabatic and advective processes and in the atmospheric thermal profile. The resulting influence on vertical velocities and precipitation affect the components of the land surface moisture and heat budgets, including soil moisture and surface temperature. The surface latent heat flux loss depends on the variation of potential evaporation and amount of soil moisture, with soil moisture change being usually the more important factor.

The solar flux change for either experiment has opposite signs at the top of the atmosphere and surface, a feature that distinguishes them from earlier GCM solar experiments [e.g., *Charney et al.*, 1977]. The fact that the results of I–III (Table 3) are, for the most part, opposite in sign to those of

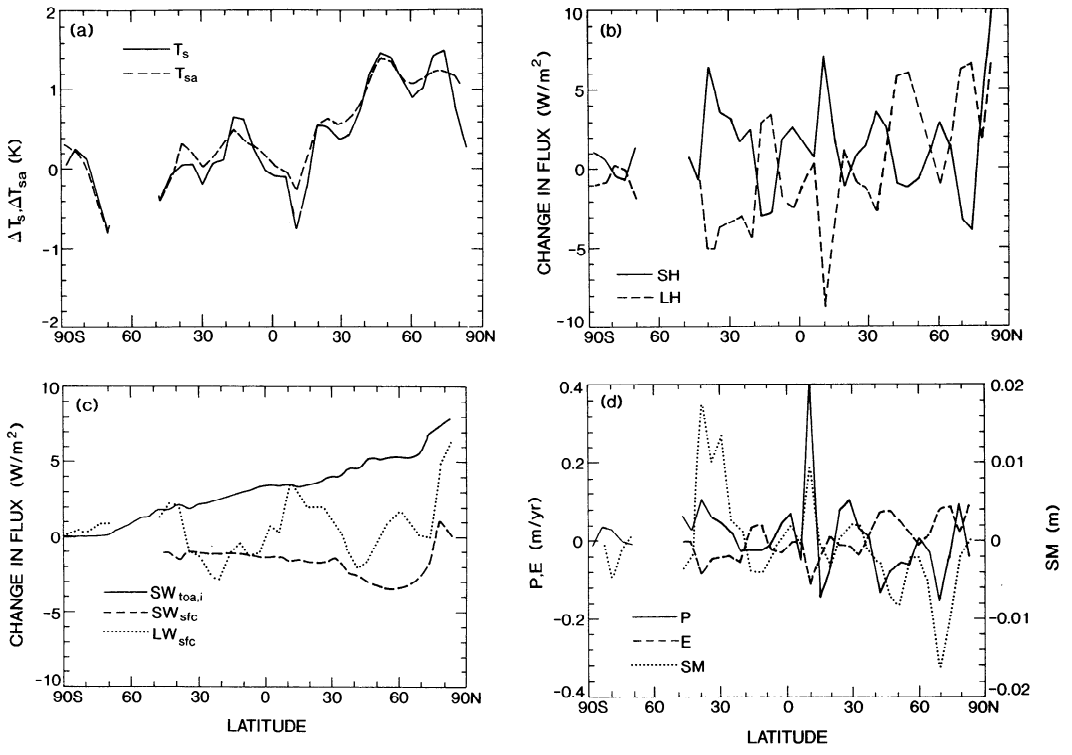

Figure 8. Zonal mean changes (methods I–III) in the GCM (June, July, August averages): (a) surface temperature (T_s) and surface air temperature (T_{sa}); (b) surface sensible heat (SH) and latent heat flux (LH); (c) initial solar radiative flux at the top of the atmosphere ($SW_{toa,i}$), net surface solar radiative flux (SW_{sfc}), and net surface longwave radiative flux (LW_{sfc}); (d) precipitation (P), evaporation (E), and soil moisture (SM).

III–IV, just like the initial solar flux differences, attributes a degree of consistency to the present model simulation of the changes in atmosphere-land surface variables and the associated physical processes. The results in Table 3 raise a caution about interpreting land surface temperature changes from considerations of only the top-of-the-atmosphere solar flux perturbations.

The limited scope of the present study inhibits an assessment of the climatic significance of the changes obtained in the heat and moisture budget components. Rather, the results highlight the significance of the vapor and drop effects and illustrate how biases in solar cloud radiative transfer can affect the simulation of the atmosphere-land surface interactions and lead to alterations in the surface heat and moisture balance. Quantitative aspects of the problem could well depend on the characteristics (e.g., physical parameterizations) of the GCM employed. The changes in the various components of the surface heat budget can be as large in magnitude as, if not more than, the solar flux changes. Further, even if the solar radiative flux biases over the midlatitude and the tropical land areas are similar, the manner in which the surface heat (including surface temperature) and moisture balances are rearranged in the regions can be quite different.

5. Summary

An empirical broadband parameterization for the shortwave characteristics of low clouds has been developed. It is easily incorporated in current GCMs and accounts for the solar radiative interactions involving water drops, in-cloud and above-cloud vapor. Because of the bases of the parameterization the present application is limited to low-lying water clouds. One virtue of the method is that it has been possible to consider variation in only two parameters among the many that are physically possible. The parameterization demonstrates that the solar radiative characteristics of low clouds can be reliably described in terms of cloud effective radius, liquid water path, and the in-cloud vapor amount. It is however necessary to include the above-cloud vapor absorption in some approximate sense when the drop radiative properties in the inhomogeneous atmosphere are computed. The parameterization employs *Slingo*'s [1989] drop single-scattering representation and provides efficient but accurate estimates of the cloud reflection, transmission, and absorption for a wide range of cases. One limitation of the present parameterization is that cloud geometrical thicknesses substantially greater (namely, with higher in-cloud water vapor) than those considered in the development of the approximation, could lead to relatively larger errors.

Comparisons with other broadband parameterizations reported in the literature indicate that deficiencies in the representation of the vapor and drop optical properties and the vapor-drop solar interactions lead to discrepancies in the solar fluxes. Compared to the present broadband cloud parameterization, the neglect of the influence of both the above-cloud and the in-cloud vapor acts to reduce the low-cloud layer absorption in the tropical regions and to increase it at middle and high latitudes. If the additional

absorption due to the in-cloud vapor is accounted for, the differences in cloud absorption occur mainly at the middle and high latitudes. The assumption of conservative scattering for water drops leads to a significant underestimate of the low-cloud absorption at most latitudes. Thus the above-cloud and in-cloud vapor and the drops play an important role in determining the solar flux absorbed by the surface and the surface-atmosphere system.

GCM simulations with fixed cloud amounts and sea surface temperatures (SSTs) have been used to investigate the significance of the vapor and drop optical properties and the manner in which the differences in the low-cloud solar radiative treatment affect the land surface heat and moisture balance. Different assumptions of the solar radiative interactions with drops and vapor in low clouds affect the cloud layer and the atmospheric absorption and result in solar flux differences at the top of the atmosphere and surface. The changes comprise a rearrangement of the solar flux absorbed by the atmosphere and surface. In this study, the sign of the solar flux difference at the surface is opposite to that at the top of the atmosphere. This feature differs in character from earlier albedo perturbation experiments [e.g., *Charney et al.*, 1977; *Coakley and Cess*, 1985].

In response to the solar flux differences the atmospheric adjustments in the adiabatic and advective processes are accompanied by changes in vertical velocity and precipitation. The latter become important in determining the surface heat (e.g., latent and sensible heat fluxes) and moisture (e.g., soil moisture, evaporation) budgets, including the land surface temperature. For example, using a broadband treatment of cloud absorption that assumes drop absorption only in the cloud layer, the surface temperatures in the United States and Europe-Asia land masses are more than 1 K warmer (exceeding the model's standard deviation) than those obtained from the assumption of vapor absorption only in the cloud layer. Thus different treatments of the vapor-drop interactions lead to distinctly different thermal fields over the continental regions. While the tropospheric temperature changes follow the solar flux differences at the top of the atmosphere in a rather obvious manner, the surface changes involve, in addition, the land surface processes and their interactions with the atmosphere's thermal, dynamical, and hydrological adjustments. Thus the land surface temperature changes do not have so simple an association with the top-of-the-atmosphere solar flux differences.

In this study, the net solar flux change due to the different broadband parameterizations at the top of the atmosphere and the surface amount to ≤ 5 W m^{-2}. The magnitude of the flux change in other energy components can be comparable to or even exceed the initial solar flux changes (e.g., surface latent heat loss). Thus even small inaccuracies in solar cloud broadband parameterizations lead to changes in low-level convergence and vertical velocity that trigger changes in the precipitation and surface moisture budgets. In turn, these alter the surface energy budget and the land surface temperature. The character of the atmosphere-land surface energy and moisture interactions varies from one geographical region to another, even if the shortwave flux changes are similar over the various regions. In particular, the changes in the vertical velocity to a solar radiative bias in the midlatitudes differs from that in the tropics; this results in dissimilar adjustments in the land surface heat and moisture components for these two regions.

By examining the relative impacts due to different cloud parameterizations on the land surface heat and moisture balance, the GCM simulations demonstrate the sensitivity of the climate system to vapor and drop optical properties and underscore the need for accuracy in the treatment of the solar cloud radiative processes. While the GCM experiments here held the SSTs and cloud cover fixed, it would be of interest to pursue similar experiments in a model with a mixed layer ocean and an interactive cloud prediction scheme. The conclusion here that the atmosphere and the land surface system are sensitive to solar cloud radiative deficiencies is applicable to other potential causes of such biases as well, e.g., uncertainties in cloud microphysical properties and the possible anomalous absorption in cloudy atmospheres, since in these instances, too, differences arise in the solar fluxes absorbed by the surface and the atmosphere.

Appendix: Derivation of VFT and VFR

VFT and VFR are parameterized using equations (1)–(6). First we use Slingo's tabulation of single-scattering properties and the LBL + DE method (RF1) to compute reference results that include water vapor and drop optical properties (i.e., $T_{\mathrm{LBL+DE}}$ and $R_{\mathrm{LBL+DE}}$). For the spectral range below 2500 cm^{-1} (which was not included in Slingo's parameterization), the drop single-scattering parameters are obtained as in RF2. Then, the drop reflectivity and transmissivity (i.e., $R_{l,\mathrm{drop}}$ and $T_{l,\mathrm{drop}}$) are calculated using the incident solar flux at the top of the cloud, as obtained from the LBL + DE result (equations (2) and (5)). Using (1) and (4), VFT and VFR are derived for each of 72 cloud cases (section 2). In the derivation the cloud drop optical depth τ is varied from 0.625 to 160, while the in-cloud vapor W is varied from 2.26 to 20.85 kg m^{-2}. Solar zenith angle is fixed at 53°, surface albedo is zero, and cloud top is at 800 mbar in a midlatitude summer atmosphere [*McClatchey et al.*, 1972]. A least squares fit is employed to obtain the empirical dependence of VFT and VFR on τ_{drop} and W as follows:

$$\begin{aligned}\mathrm{VFT} = {} & a_1 + a_2\tau + a_3 W + a_4\tau^2 + a_5 W^2 + a_6\tau^3 + a_7 W^3 \\ & + a_8\tau^4 + a_9 W^4 + a_{10} W\tau + a_{11} W\tau^2 + a_{12} W^2\tau \\ & + a_{13} W\tau^3 + a_{14} W^2\tau^2 + a_{15} W^3\tau \end{aligned} \quad \text{(A1)}$$

Table A1. Coefficients a_i and b_i in equations (A1) and (A2)

i	a_i	b_i
1	1.004465	0.983270
2	0.010451	0.007899
3	−0.065975	0.022400
4	−0.072845	−0.003964
5	0.014006	−0.031112
6	0.088795	0.003035
7	0.000965	0.009529
8	−0.034544	−0.000244
9	−0.000122	−0.000871
10	−0.018128	0.013829
11	0.007729	−0.040609
12	−0.001909	0.018926
13	−0.000398	0.010768
14	0.001938	0.000307
15	−0.000562	−0.004280

The relative error due to the fits (equations (A1) and (A2)) is less than 1%.

$$\mathrm{VFR} = b_1 + b_2\tau + b_3 W + b_4\tau^2 + b_5 W^2 + b_6\tau^3 + b_7 W^3 + b_8\tau^4 + b_9 W^4 + b_{10} W\tau + b_{11} W\tau^2 + b_{12} W^2\tau + b_{13} W\tau^3 + b_{14} W^2\tau^2 + b_{15} W^3\tau \quad \text{(A2)}$$

where $\tau = \log_{10}(\tau_{\mathrm{drop}})$ and a_i, b_i ($i = 1, 15$) are coefficients listed in Table A1.

References

Charney, J. G., W. J. Quirk, S. H. Chow, and J. Kornfield, A comparative study of the effects of albedo change on drought on semi-arid region, *J. Atmos. Sci.*, *34*, 1366–1385, 1977.

Chen, C.-T., Sensitivity of the simulated global climate to perturbations in low cloud microphysical properties, Ph.D. thesis, 279 pp., Princeton Univ., N. J., 1994.

Coakley, J. A., Jr., and R. D. Cess, Response of the NCAR community climate model to the radiative forcing by the naturally occurring tropospheric aerosol, *J. Atmos. Sci.*, *42*, 1677–1692, 1985.

Coakley, J. A., Jr., R. D. Cess, and F. B. Yurevich, The effect of tropospheric aerosols on the earth radiation budget: A parameterization for climate models, *J. Atmos. Sci.*, *40*, 116–138, 1983.

Held, I. M., Stationary and quasi-stationary eddies in the extratropical troposphere: Theory, in *Large-Scale Dynamical Processes in the Atmosphere*, edited by B. J. Hoskin and R. P. Pearce, pp. 127–168, Academic, San Diego, Calif., 1983.

Joseph, J. H., W. Wiscombe, and J. A. Weinman, The delta-Eddington approximation for radiative flux transfer, *J. Atmos. Sci.*, *33*, 2452–2459, 1976.

Lacis, A. A., and J. E. Hansen, A parameterization of the absorption of solar radiation in the Earth's atmosphere, *J. Atmos. Sci.*, *31*, 118–133, 1974.

Lofgren, B. M., Sensitivity and feedback associated with vegetation-related land surface parameters in a general circulation model, Ph.D. thesis, 206 pp., Princeton University, N. J., 1993.

Manabe, S., and A. J. Broccoli, A comparison of climate model sensitivity with data from the last glacial maximum, *J. Atmos. Sci.*, *23*, 2643–2651, 1985.

Mason, B. J., *The Physics of Cloud*, 672 pp., Clarendon, Oxford, 1971.

McClatchey, R. A., R. W. Fenn, J. E. A. Selby, F. E. Volz, and J. S. Garing, Optical properties of the atmosphere, *AFCRL Rep. AFCRL-72-0497*, 110 pp., Hanscom Air Force Base, Bedford, Mass., 1972.

Ramaswamy, V., and C.-T. Chen, An investigation of the global solar radiative forcing due to changes in the cloud liquid water path, *J. Geophys. Res.*, *98*, 16,703–16,712, 1993.

Ramaswamy, V., and S. M. Freidenreich, Solar radiative line-by-line determination of water vapor absorption and water cloud extinction in inhomogeneous atmospheres, *J. Geophys. Res.*, *96*, 9133–9157, 1991.

Ramaswamy, V., and S. M. Freidenreich, A study of broadband parameterizations of the solar radiative interactions with water vapor and water drops, *J. Geophys. Res.*, *97*, 11,487–11,512, 1992.

Rossow, W. B., and A. A. Lacis, Global, seasonal cloud variations from satellite radiance measurements, II, Cloud properties and radiative effects, *J. Clim.*, *3*, 1204–1253, 1990.

Slingo, A., A GCM parameterization of the shortwave radiative properties of water cloud, *J. Atmos. Sci.*, *46*, 1419–1427, 1989.

Stephens, G. L., Optical properties of eight water cloud types, *Div. Atmos. Phys. Tech. Pap. 36*, Commonwealth Sci. and Ind. Res. Organ., Aspendale, Australia, 1979.

C.-T. Chen and V. Ramaswamy (corresponding author), NOAA Geophysical Fluid Dynamics Laboratory, P. O. Box 308, Princeton, NJ 08542.

(Received June 27, 1994; revised January 12, 1995; accepted February 10, 1995.)